Spring 2021

A Numerical Investigation of Fractional Models for Viscoelastic Materials With Applications on Concrete Subjected to Extreme Temperatures

Murray Macnamara

A Numerical Investigation of Fractional Models for Viscoelastic Materials with Applications on Concrete Subjected to Extreme Temperatures

by

Murray Macnamara

Bachelor of Science
Augusta University, 2015

Submitted in Partial Fulfillment of the Requirements

for the Degree of Master of Science in

Mathematics

College of Arts and Sciences

University of South Carolina

2021

Accepted by:

Hong Wang, Director of Thesis

Xinfeng Liu, Reader

Tracey L. Weldon, Interim Vice Provost and Dean of the Graduate School

Acknowledgments

This thesis is the final product of a dream that has been thought of for many years once graduating from Augusta University with my Bachelors in Physics and Mathematics. Taking a few years off to determine what I would intend to study for my masters lead to many drawn out conversations with people dear to me, until finding myself in a fortunate situation of being located in Columbia, SC with the prestigious University of South Carolina campus nearby. At that time my family and partner urged me to finish my goal of higher education, and soon I was granted admission into the Masters of Sciences program for Applied Mathematics at USC. It was rough going back to school after three years, however the understanding and patience given to me by my peers and professors supported me along my journey. It was not easy in the slightest, however being inspired by the faith my grandparents and partner had in me I was able to overcome many obstacles. To that end I would like to extend my greatest thanks and appreciation to Harrison Pitts, Mitchell Toomey, Erica Battle, and Tom and Sharon Macnamara, who acted as my supporting backbone throughout this journey. My coworkers among the Laguna Tools SC office, who supported my academic goals during the entirety of my collegiate experience, as well as Yiqun Li, Dr. Hong Wang, and Dr. Xinfeng Liu for their continued patience and guidance. Lastly I will thank the ARO under MURI Grant W911NF-15-1-0562 and the National Science Foundation under Grants DMS-1620194 and DMS-2012291 for their support for this project and projects like these. Without the financial help they provide many students would not be able to study so fervently to achieve their dreams.

Abstract

Materials exhibiting both elastic and viscous properties have been termed the name viscoelastic materials and have been modeled using a combination of integer order derivatives affixed in varying ways called viscoelastic models. This results in highly complicated numerical procedures necessitating highly expensive computational time which we will show. To that end the use of fractional derivatives were researched and determined to be the ideal solution for modeling these materials, of which this paper is focused on exploring. Such research began as a theoretical study, however over time the applied benefits were discovered and utilized and have since been expanded on, allowing the complicated numerical procedures mentioned above to be replaced with succinct numerical schemes. From these schemes we wished to focus on how to hone the numerical respect of material property contributions to the results, to which we focused on three different types of definitions for how to numerically model them, specifically the Caputo fractional derivative in this paper.

In this thesis we will first give an introduction of viscoelastic materials and the integer order models that were conceived, along with an exploration of how complicated these models can become. From there we will introduce fractional derivatives and the different definitions that exist, focusing on the Caputo fractional derivative. We will then explore the benefits of fractional viscoelastic models compared to integer order models, and from there we will expand, introduce, and compare three different definitions of variable order versions of such fractional models.

Table of Contents

List of Figures

Chapter 1

Introduction

1.1 Background

In the physical world matter can typically be described as having either primarily elastic or viscous properties. The matter that corresponds with elastic properties can be described under the study of solid mechanics, where materials subjected to an external stress return to their resting shape after the stress has been removed. Think of a spring. Matter with viscous properties are described under the study of fluid mechanics, and these are the class of materials which deform unrecognizably after an external force has been applied. However matter which can not be distinctly described as either elastic or viscous due to having properties of both garner the name viscoelastic materials. An example of such is shape-memory polymers, which achieves a temporary shape after deformation but then is able to retain its original shape after some outside stimulus such as a change in temperature. When modeling this material using standard differential equations the amount of parameters and requirement for precise calculations becomes paramount, which creates quite difficult numerical procedures. This difficulty creates a problem due to the widespread usefulness of the material, such as industrial settings ranging from the building industry to sports wear, and as medical applications including orthopedic surgery[4, 7]. Another material that displays viscoelastic properties is concrete, a material which has a high compressive strength, allowing it to resist cracking under high loads, but low tensile strength, where it cracks if it is pulled apart. The interesting facet of concrete is how

it reacts to high temperatures under constant stress, resulting in a time dependent creep. In [2] this creep is broken up into two categories, that within moderately high temperatures, and those subjected to more extreme temperatures. For the moderate temperatures there are two processes that work against each other, one being the heat which works to break the individual bonds within the solid, accelerating creep. However the heat also draws out the moisture within the concrete thus ageing it faster and decreasing the creep. Then at extreme temperatures, the concrete undergoes many microscopic bond ruptures as well as dehydration, as the moisture that was previously being drawn out slowly due to lower temperatures is now evaporating quickly. This creep is a very important subject to study due to the age of nuclear power and the reactors that are built out of concrete. We need to know how to model these materials to have a clearer understanding of how to create better equipment for our future.

1.2 Viscoelastic Models

To model these viscoelastic materials the notion of using springs and dashpots were introduced and combined in an assortment of ways. Springs model ideal elastic behavior dependent on the elastic modulus of the element, while dashpots model ideal Newtonian (viscous) fluids and depend on the viscosity of the fluid. The particular relationship that we use to model these materials focuses on the interaction between stress, σ which measures how much force is applied to an material, and strain, ϵ which measures the deformation of the material. However as viscoelastic materials possess both elastic and viscous properties just a spring or dashpot alone isn't enough to measure these unique materials, so as a result a combination of these elements are used. These building blocks can be connected in many different fashions to create many different models-all in the effort to more accurately model different types of materials. The reasoning for the combination of these elements resides in the fact

that some models may model stress relaxation resulting from constant strain well, but it may fail to model the effects of constant stress, otherwise known as creep, of the material accurately. This issue is seen conversely in other models as well. In an effort to combat these effects new models are created focusing on the addition of many different springs, dashpots, etc. until over time the general model for the subsequent linear combinations evolves into $n \in \mathbb{Z}$ different spring elements placed in some relation to $m \in \mathbb{Z}$ dashpot elements. This creates the issue of n, m unknowns just to model these materials, and as such create computationally expensive differential equations with many different unknowns.

1.3 Fractional Derivatives

There exists a solution to the problem created by the limiting integer order differential equations-one that includes the utilization of fractional order derivatives. The history of such derivatives dates back to 1695, where Leibniz pondered the existence of a half derivative to L'Hôpital in a letter[6]. Since then the study of such derivatives have been the focus of purely theoretical mathematicians until the last century when authors found the usefulness when applied to a variety of materials. This particular usefulness can be visually seen in Fig: 1.1, where the degree α of the fractional derivative $D^{\alpha}y(x)$ increases by 0.1 from the zeroth derivative of the function $y = x^2$, to the first integer order derivative $y = 2x$.

It is visible that data that may be modeled better in a space between the first and zeroth derivative of a function can be done in a seamless fashion by a single fractional derivative, instead of a linear combination of two or more integer order derivatives. There exists many different definitions for how to compute the fractional derivative, the first of which is the Riemann-Liouville fractional derivative

$$ {}_{a}^{RL}D_{t}^{\alpha} f(t) = \frac{1}{\Gamma(1-\alpha)} \frac{d}{dt} \int_{a}^{t} \frac{f(\tau)}{(t-\tau)^{\alpha}} d\tau \tag{1.1} $$

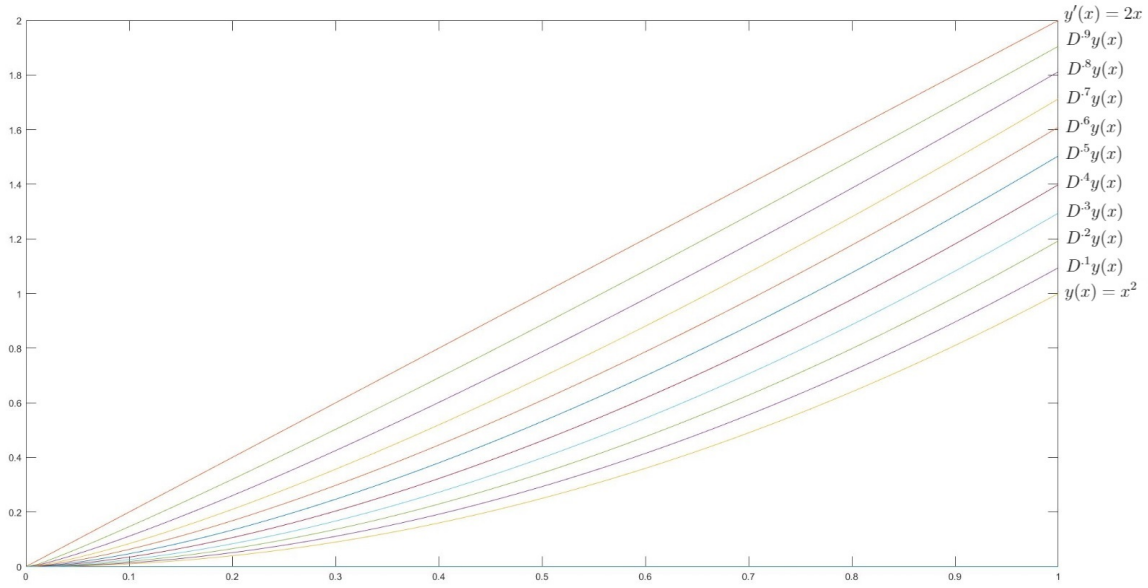

Figure 1.1: Use of Fractional Derivatives

with advantages resulting from the lack of continuity requirements at the initial time as well as lack of smoothness for the function, seen in the derivative being taken after the integration is calculated[1]. The second most widely used fractional derivative is the Caputo fractional derivative

$$ {}_a^C D_t^\alpha f(t) = \frac{1}{\Gamma(1-\alpha)} \int_a^t \frac{f'(\tau)}{(t-\tau)^\alpha} d\tau \tag{1.2} $$

which has the initial conditions and boundary restrictions prebuilt into the definition, making it particularly useful when attempting to model real world problems[1]. Other methods to take fractional derivatives include Fourier transform defined fractional derivatives which require the interval $(-\infty, \infty)$, the Grünwald-Letnikov fractional derivatives relying on summation processes, as well as several others. However due to the advantages of the Caputo fractional derivative combined with the findings of [9], where it was concluded that a time dependent α with integer limits at the boundary and initial time allows the fractional derivative to avoid the common case of singularities exhibited there, we chose the Caputo fractional derivative as the primary definition used throughout this paper. One interesting thing to note for the Riemann-Liouville and Caputo fractional derivative is the intersection at the initial condition,

where

$$ {}_0^C D_t^\alpha f(t) = {}_0^{RL} D_t^\alpha f(t) - \frac{f(0)t^{-\alpha}}{\Gamma(1-\alpha)} \tag{1.3} $$

Here it is visible that the two definitions differ only by a singular boundary term.

Chapter 2

Mathematical Models

2.1 Integer Order Models

The basic building blocks of viscoelastic materials are seen below in Fig: 2.1

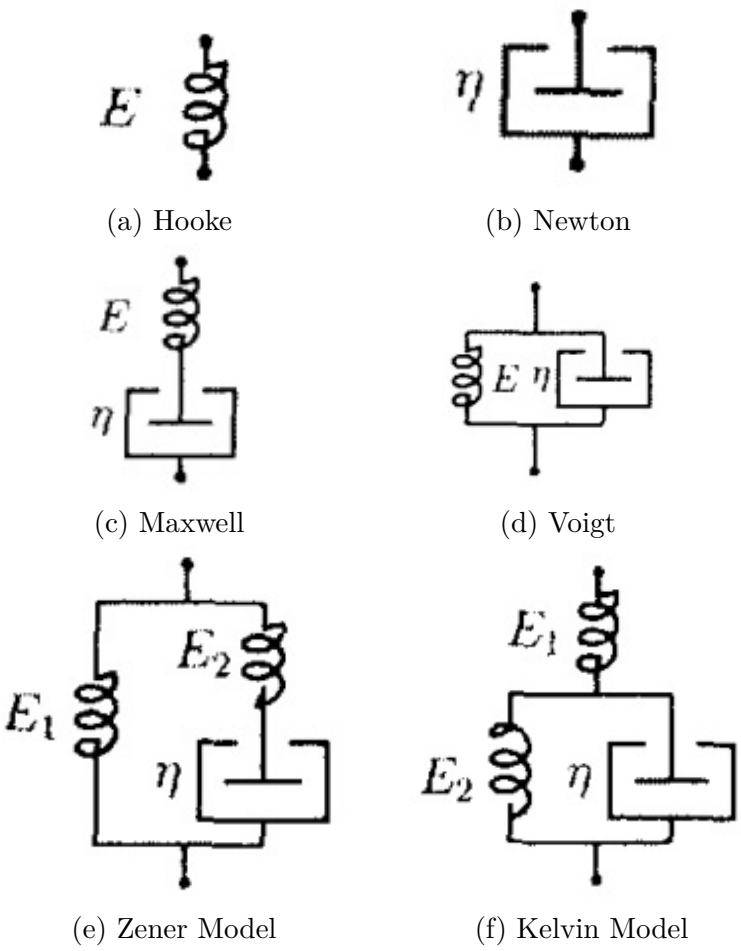

(a) Hooke (b) Newton

(c) Maxwell (d) Voigt

(e) Zener Model (f) Kelvin Model

Figure 2.1: Important components of viscoelastic modeling.

with Fig: 2.1(a) the spring mentioned earlier with elastic modulus E, and Fig: 2.1(b) the dashpot with viscosity η. The Maxwell Model (Fig: 2.1(c)) represents the

next basic step by placing a spring in series with a dashpot, while the Voigt Model (Fig: 2.1(d)) instead aligns the two elements in parallel with each other. Here it is important to note that in series components, the total strain of the system is the summation of the individual strain of the components, whereas the total stress of the system is equivalent to the individual stress of each component. The opposite is true for parallel circuits as the total strain of the system is equal to the strain of each branch, while the total stress of the system is equal to the summation of the stress through each branch. With the basic models known along with the rules governing the equations of how the stress and strain interact with each other, we can now derive the equations for each of the models presented in Fig: 2.1. The spring in Fig: 2.1(a) is described by Hooke's law with the strain and stress linearly depending on each other with elastic modulus E, seen in Eq (2.1)

$$\sigma(t) = E\epsilon(t) \tag{2.1}$$

while the dashpot in Fig: 2.1(b) is represented in Eq (2.2) by the linear relationship between stress and the time derivative of strain with viscosity η

$$\sigma(t) = \eta\frac{d\epsilon(t)}{dt} \tag{2.2}$$

As stated previously these two elements alone are not enough to model the materials this paper is focused on, and as such the next building block to create is the Maxwell model from Fig: 2.1(c). Using Eq (2.1) with σ_s, ϵ_s representing the stress and strain respectively, and Eq (2.2) using instead σ_d, ϵ_d, we differentiate the equation relating the total strain ϵ_{tot} to the spring and dashpot element to get

$$\frac{d\epsilon_{tot}}{dt} = \frac{d\epsilon_s}{dt} + \frac{d\epsilon_d}{dt}$$

As we have a series circuit we know that

$$\sigma_{tot} = \sigma_s = \sigma_d$$

which is substituted into our Eq (2.1) and Eq (2.2) and rearranged to solve for our strain derivative to obtain

$$\frac{d\epsilon_{tot}}{dt} = \frac{1}{E}\frac{d\sigma_{tot}}{dt} + \frac{\sigma_{tot}}{\eta} \tag{2.3}$$

thus finalizing our Maxwell model equation. Our next fundamental building block is the Voigt model seen in Fig: 2.1(d). As this is a parallel circuit we know that

$$\sigma_{tot} = \sigma_s + \sigma_d$$

$$\epsilon_{tot} = \epsilon_s = \epsilon_d$$

so substituting in our Eq (2.1) and Eq (2.2), we get our final equation for the Voigt model seen below.

$$\sigma_{tot} = E\epsilon_{tot} + \eta\frac{d\epsilon_{tot}}{dt} \tag{2.4}$$

Setting σ as a constant and solving the resulting differential equations in order to model creep, we see the Maxwell model results in a linear equation which is bad, while the Voigt model results in an exponential decay equation which models creep well. However to achieve stress relaxation we need to set ϵ as a constant and solve those resulting differential equations, and we see the opposite is true of the models here. To combat this the Zener model is introduced see in Fig: 2.1(e) which places the Maxwel model in a parallel circuit with a spring. For this equation we have

$$\sigma_{tot} = \sigma_1 + \sigma_m$$

$$\epsilon_{tot} = \epsilon_1 = \epsilon_m$$

where $\sigma_{tot}, \epsilon_{tot}$ is the total stress/strain of the model, σ_1, ϵ_1 is the stress/strain through E_1, and σ_m, ϵ_m is the stress/strain through the Maxwell element. The relations of the Maxwell element are as follows

$$\sigma_m = \sigma_2 = \sigma_d$$

$$\epsilon_m = \epsilon_2 + \epsilon_d$$

with σ_2, ϵ_2 representing the stress, strain of the spring in the Maxwell element and σ_d, ϵ_d the stress, strain of the dashpot. Rearranging these equations and substituting

Eq's (2.1) and (2.2) we arrive at the final equation

$$\frac{E_2}{\eta}\sigma_{tot} + \frac{d\sigma_{tot}}{dt} = \frac{E_1 E_2}{\eta}\epsilon_{tot} + (E_1 + E_2)\frac{d\epsilon_{tot}}{dt} \tag{2.5}$$

While this model provides a good qualitative description, it leaves the quantitative description lacking[6]. Thus leading to the Kelvin model, where the Voigt element is placed in series with a spring, seen in Fig: 2.1(f). From this placement we know

$$\sigma_{tot} = \sigma_1 = \sigma_v$$

$$\epsilon_{tot} = \epsilon_1 + \epsilon_v$$

where $\sigma_{tot}, \epsilon_{tot}$ is the total stress/strain of the model, σ_1, ϵ_1 is the stress/strain through E_1, and σ_v, ϵ_v is the stress/strain through the Voigt element. Focusing on the Voigt element we have

$$\sigma_v = \sigma_2 + \sigma_d$$

with σ_2 representing the stress through E_2 of the Voigt element, and σ_d the stress through the dashpot. Rearranging and substituting in Eq's (2.1) and (2.2) to solve for ϵ_{tot} and σ_{tot}, we obtain

$$E_1\left[\frac{E_2}{\eta}\epsilon_{tot} + \frac{d\epsilon_{tot}}{dt}\right] = \frac{(E_1 + E_2)}{\eta}\sigma_{tot} + \frac{d\sigma_{tot}}{dt}$$

Similar to the Zener model, this model provides a good description of viscoelastic models, but is unable to model the materials well[6]. In an effort to fine tune these models to match the experimental results from different types of viscoelastic materials, it was found that the highest level of accuracy was to keep adding on dashpots and springs in either parallel or series connections, an example of which can be seen in the Generalized Maxwell model, Fig: 2.2.

The equations that are known for this model as a whole are

$$\sigma_{tot} = \sigma_{eq} + \sum_{i=1}^{N} \sigma_i^m$$

$$\epsilon_{tot} = \epsilon_{eq} = \epsilon_1^m = ... = \epsilon_N^m$$

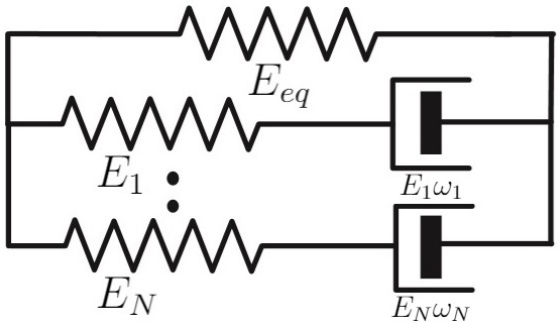

Figure 2.2: Generalized Maxwell model

with the individual elements of each branch having the relations below

$$\begin{aligned} \sigma_i^m &= \sigma_i^e = \sigma_i^\omega \\ \epsilon_i^m &= \epsilon_i^e + \epsilon_i^\omega \\ \sigma_i^e &= E_i \epsilon_i^e \\ \sigma_i^\omega &= E_i \omega_i \frac{d\epsilon_i^\omega}{dt} \end{aligned} \tag{2.6}$$

where $\sigma_{tot}, \epsilon_{tot}$ is the total stress/strain for the model as a whole, $\sigma_{eq}, \epsilon_{eq}$ the stress/strain for the first elastic branch, and $\sigma_i^m, \epsilon_i^m, \sigma_i^e, \epsilon_i^e, \sigma_i^\omega, \epsilon_i^\omega$ the stresses/strains for the i'th Maxwell branches. Rearranging these equations we derive the fractional damping element found in [3], seen below

$$\begin{aligned} E_i \omega_i \frac{d\epsilon_i^\omega}{dt} = \sigma_i^\omega = \sigma_i^e = E_i \epsilon_i^e \\ \frac{d\epsilon_i^\omega}{dt} = \frac{\epsilon_{tot} - \epsilon_i^\omega}{\omega_i} \end{aligned} \tag{2.7}$$

which represents the damping element of the individual Maxwell elements of the Generalized Maxwell model. To find the value for our σ_m we take the equations above and substitute in our ϵ_{tot} for our ϵ_i^m and we get the equation

$$\epsilon_{tot} = \epsilon_i^e + \epsilon_i^\omega \tag{2.8}$$

which we take the derivative of to get the equation

$$E_i \frac{d\epsilon_{tot}}{dt} = \frac{d\sigma_i^m}{dt} + \frac{\sigma_i^m}{\omega_i}$$

From here we just solve the differential equation for σ_i^m assuming ϵ_{tot} is constant, representing stress relaxation. With the initial condition $\sigma_i^m|_{t=0} = E_i\epsilon_{tot}$ given from our relationship found in Eq (2.6), which we plug in our earlier derived relationship Eq (2.7) we get our final Generalized Maxwell equation,

$$\sigma_{tot} = \epsilon_{tot}E_{eq} + \sum_{i=1}^{N} E_i\epsilon_{tot}e^{\frac{-t}{\omega_i}} \tag{2.9}$$

The procedure for finding the values for the spring modulus E_i seen in Eq (2.9) is explained in [8], and this is one example of a viscoelastic model with many unknown parameters. To expand on this even more dashpots and springs are added, until a generalized model can be represented by the equation below

$$\sum_{k=0}^{n} a_k \frac{d^k\sigma}{dt^k} = \sum_{k=0}^{m} b_k \frac{d^k\epsilon}{dt^k}$$

where $k, n, m \in \mathbb{Z}$ and the highest level of accuracy is achieved when $n = m$. In spite of that it became apparent that to more finely tune these models the values of n, m, k eventually become so high resulting in highly complicated differential equations featuring many unknowns.

2.2 Fractional Models

A solution exists, starting with a simple springpot represented by Eq (2.10)

$$\sigma = E\omega^\alpha \frac{d^\alpha\epsilon}{dt^\alpha} \tag{2.10}$$

as it will act as our primary fractional element in our models with ω representing the relaxation time of the springpot[8]. When $\alpha = 1$, we set $E\omega = \eta$ to acquire our traditional dashpot equation stated above in Eq (2.2), and when $\alpha = 0$ we have our traditional spring equation seen in Eq (2.1). For our fractional equivalent to our Maxwell model we simply substitute Eq (2.10) for our dashpot equation used before and retain the same relationships of strain and stress for the spring and springpot

placed in series

$$\sigma_{tot} = \sigma_s = \sigma_\omega$$

$$\epsilon_{tot} = \epsilon_s + \epsilon_\omega$$

We will define $\sigma_{tot}, \epsilon_{tot}$ as the total stress and strain through the Maxwell model, and σ_s, ϵ_s, $\sigma_\omega, \epsilon_\omega$ as the stress, strain through the spring and springpot element respectively. With these established, we can derive the fractional Maxwell equation by substituting and rearranging Eq's (2.1) and (2.10) to solve ϵ_{tot} in terms of σ_{tot}.

$$\begin{aligned} \sigma_{tot} &= E\omega^\alpha \frac{d^\alpha \epsilon_\omega}{dt^\alpha} \\ \sigma_{tot} &= E\omega^\alpha \frac{d^\alpha (\epsilon_{tot} - \epsilon_s)}{dt^\alpha} \\ \sigma_{tot} &= E\omega^\alpha \left[\frac{d^\alpha \epsilon_{tot}}{dt^\alpha} - \frac{1}{E} \frac{d^\alpha \sigma_{tot}}{dt^\alpha} \right] \\ \frac{d^\alpha \epsilon_{tot}}{dt^\alpha} &= \frac{1}{E} \frac{d^\alpha \sigma_{tot}}{dt^\alpha} + \frac{\sigma_{tot}}{E\omega^\alpha} \end{aligned} \tag{2.11}$$

It is clear that Eq (2.11) is equivalent to Eq (2.3) under the same restrictions of the equivalency of Eq (2.10) to Eq (2.2). For our fractional Voigt model the same holds true from our Eq (2.4) for our relations of our stress, strain in parallel

$$\sigma_{tot} = \sigma_s + \sigma_d$$

$$\epsilon_{tot} = \epsilon_s = \epsilon_d$$

Substituting in our Eq (2.1) and Eq (2.10), we get our fractional equation for the Voigt model seen below.

$$\sigma_{tot} = E\epsilon_{tot} + E\omega^\alpha \frac{d^\alpha \epsilon_{tot}}{dt^\alpha} \tag{2.12}$$

As the Caputo fractional derivative is a linear operator our fractional equations for our models look nearly identical, with the exception of our springpot replacing the traditional dashpot. For our more complex models there is a little more work to do, starting with the Kelvin model we have

$$\sigma_{tot} = \sigma_1 = \sigma_v$$

$$\epsilon_{tot} = \epsilon_1 + \epsilon_v$$

where $\sigma_{tot}, \epsilon_{tot}$ is the total stress/strain of the model, σ_1, ϵ_1 is the stress/strain through E_1, and σ_v, ϵ_v is the stress/strain through the Voigt element the spring is in series with. Looking closer at the Voigt element we have

$$\sigma_v = \sigma_2 + \sigma_\omega$$

with σ_2 representing the stress through E_2 of the Voigt element, and σ_ω the stress through the springpot. Rearranging and substituting in Eq's (2.1) and (2.10) using our viscosity constant η to solve for ϵ_{tot} and σ_{tot}, we get

$$E_1 \left[\frac{E_2}{\eta} \epsilon_{tot} + \frac{d^\alpha \epsilon_{tot}}{dt^\alpha} \right] = \frac{(E_1 + E_2)}{\eta} \sigma_{tot} + \frac{d^\alpha \sigma_{tot}}{dt^\alpha}$$

The model we will use quite a bit in our paper will be the Fractional Zener model, seen in Fig: 2.3. The main difference to note between Fig: 2.1(e) and Fig: 2.3 is that the springpot has the relaxation time constant ω represented, with $\eta = E_{neq}\omega^\alpha$.

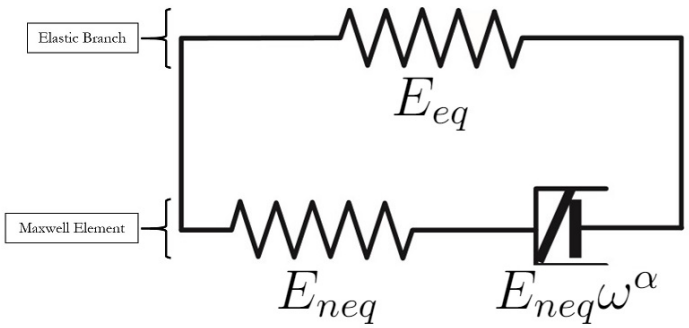

Figure 2.3: Fractional Zener model

Here we need to derive an equation to model how the total stress (σ_{tot}) responds to different types of strain (ϵ_{tot}). We know for the Elastic branch Eq (2.1) with σ_e the stress response of the elastic spring, E_{eq} the equilibrium elastic modulus, and ϵ_e the strain. The equations that are known for the Zener model as a whole and the

Maxwell element are

$$\begin{aligned} \sigma_{tot} &= \sigma_m + \sigma_e \\ \epsilon_{tot} &= \epsilon_m = \epsilon_e \\ \sigma_m &= \sigma_n = \sigma_\omega \\ \epsilon_m &= \epsilon_n + \epsilon_\omega \end{aligned} \tag{2.13}$$

Here $\sigma_m, \epsilon_m,\ \sigma_n, \epsilon_n,\ \sigma_\omega, \epsilon_\omega$ are the stress responses and strain for the Maxwell element, the non-equilibrium elastic response, and the springpot respectively. For the fractional version of our damping element derived in Eq (2.7), we have

$$\frac{d^\alpha \epsilon_\omega}{dt^\alpha} = \frac{\epsilon_{tot} - \epsilon_\omega}{\omega^\alpha} \tag{2.14}$$

Rearranging our known equations along with Eq (2.13) and Eq (2.14), we found Eq (2.15) for σ_{tot} in terms of ϵ_{tot}

$$\sigma_{tot} + \omega^\alpha \frac{d^\alpha \sigma_{tot}}{dt^\alpha} = E_{eq}\epsilon_{tot} + \omega^\alpha (E_{neq} + E_{eq}) \frac{d^\alpha \epsilon_{tot}}{dt^\alpha} \tag{2.15}$$

In [8] they conducted many different experiments comparing this Fractional Zener model to the Generalized Maxwell model seen in Fig: 2.2 and it was shown that these two models have near identical results. It is clear that the inclusion of fractional derivatives into these viscoelastic models create a clear advantage to the previous integer ordered models, in part due to the fact that while Eq (2.9) exhibits decay based on the exponential factor in the summation thus requiring many parameters, Eq (2.15) decays according to power law decay with very few parameters.

2.3 Variable Order Fractional Models

While constant order viscoelastic models suffice for the purpose of verifying the equivalence of the Fractional Zener model and the Generalized Maxwell model, in [2] it is shown that concrete subjected to constant stress exhibit varying creep behavior

Table 2.1: Parameters used for our Eq's (3.4), (3.6), and (3.8) with $\eta =$ x10^4MPa*min$^\alpha$

	Calcareous		Siliceous Aggregate	
f'$_c$	23.2Mpa		22.2Mpa	
Temp(°F):	α	η	α	η
71.6	0.450	80.0	0.250	40.0
399.2	0.385	24.5	0.377	15.5
600.8	0.410	15.5	—	—
800.6	0.460	10.5	0.345	4.9
1000.4	0.420	7.8	0.260	1.9
1200.2	0.373	2.8	—	—

based on the external temperature of its surroundings, with both α and η exhibiting temperature dependency seen in Table 2.1. As such equations were constructed for T, α, and η to model this dependency on time and temperature for calcareous aggregate as seen in Eq (2.16)

$$
\begin{aligned}
&T = 71.6 + 3.51t \\
&T < 600^\circ F \\
&\quad \alpha = -5.36\text{x}10^{-10}(T - 759.6741)^3 - 7.849\text{x}10^{-11}T^2 + 2.53\text{x}10^{-4}T + 0.257 \\
&\quad \eta = 2.3382(T - 596.2261)^2 + 1.55\text{x}10^5 \\
&T \geq 600^\circ F \\
&\quad \alpha = 1.73\text{x}10^{-9}(T + 931.86)^3 - 1.01\text{x}10^{-5}T^2 + 5.7883\text{x}10^{-4}T - 2.5093 \\
&\quad \eta = 9.3568\text{x}10^{-4}(T - 900)^3 - 127.43333T + 204600
\end{aligned}
\tag{2.16}
$$

with those for siliceous aggregate found in Eq (2.17)[2].

$$
\begin{aligned}
&T = 71.6 + 3.006t \\
&\alpha = 5.7323\text{x}10^{-11}(T - 677.8124)^3 - 5.9015\text{x}10^{-7}T^2 + 6.3136\text{x}10^{-4}T \\
&\qquad + 0.2201 \\
&T < 800^\circ F \\
&\quad \eta = 495020e^{-0.0029T} \\
&T \geq 800^\circ F \\
&\quad \eta = 0.1985(T - 1270)^2 + 5000
\end{aligned}
\tag{2.17}
$$

Due to T varying in time we rewrite the springpot from Eq (2.10) as

$$\frac{d^{\alpha(T(t))}\epsilon(t)}{dt^{\alpha(T(t))}} = \frac{\sigma}{\eta(T(t))} \tag{2.18}$$

From this springpot definition we wanted to explore three different definitions of how to incorporate the variable α into the formulation process[5]. Here we will set $\alpha(T(t)) = \alpha(T(t,\tau))$, with t representing what we are taking the fractional derivative with respect to and τ being our integration variable. We wish to explore how altering the α's t, τ dependency transforms our final resulting graph, which is visually explored in Chapter 4 by focusing on how this change in our α equation redefines our Eq (1.2), with us defining the impulse function $h(t,\tau)$ as

$$h(t,\tau) = \frac{1}{\Gamma(1 - \alpha(T(t,\tau)))(t-\tau)^{\alpha(T(t,\tau))}} \tag{2.19}$$

2.3.1 Definition 1: $\alpha(T(t,\tau)) \Rightarrow \alpha(T(t))$

We will define our standard Caputo fractional derivative with respect to the temperature dependent α as Eq (2.20), with our impulse function as well.

$$
\begin{aligned}
{}_0^1D_t^{\alpha(T(t))}\epsilon(t) &= \frac{1}{\Gamma(1 - \alpha(T(t)))}\int_0^t \frac{\epsilon'(\tau)}{(t-\tau)^{\alpha(T(t))}}d\tau \\
h(t,\tau) &= \frac{1}{\Gamma(1 - \alpha(T(t)))(t-\tau)^{\alpha(T(t))}}
\end{aligned}
\tag{2.20}
$$

Here our $\alpha(T(t))$ is seen as a constant function as the integration within the derivative is with respect to τ.

2.3.2 Definition 2: $\alpha(T(t,\tau)) \Rightarrow \alpha(T(\tau))$

Due to the dependence of our α function on τ, the derivative as a whole is able to retain the memory of the function as it evolves over time. As such the second definition for our Caputo fractional derivative is seen in Eq (2.21)

$$\begin{aligned} {}_0^2D_t^{\alpha(T(t))}\epsilon(t) &= \int_0^t \frac{\epsilon'(\tau)}{\Gamma(1-\alpha(T(\tau)))(t-\tau)^{\alpha(T(\tau))}}d\tau \\ h(t,\tau) &= \frac{1}{\Gamma(1-\alpha(T(\tau)))(t-\tau)^{\alpha(T(\tau))}} \end{aligned} \tag{2.21}$$

Immediately it is seen that this definition will produce different results, however to fine tune the addition of the memory aspect that our α function can now store, we will look at our next definition by incorporating t, τ to interact with each other.

2.3.3 Definition 3: $\alpha(T(t,\tau)) \Rightarrow \alpha(T(t-\tau))$

Our third definition relies on taking the difference between the integration variable and the t value

$$\begin{aligned} {}_0^3D_t^{\alpha(T(t))}\epsilon(t) &= \int_0^t \frac{\epsilon'(\tau)}{\Gamma(1-\alpha(T(t-\tau)))(t-\tau)^{\alpha(T(t-\tau))}}d\tau \\ h(t,\tau) &= \frac{1}{\Gamma(1-\alpha(T(t-\tau)))(t-\tau)^{\alpha(T(t-\tau))}} \end{aligned} \tag{2.22}$$

creating a reliant relationship of our α function to both our t and our τ. In Chapter 4 we will look further into how this affects the impulse functions, proving that Eq's (2.21) and (2.22) create a system that evolves with time, so that the derivative is weighted by the material properties in our α function, producing a smoother graph.

Chapter 3

Numerical Schemes

3.1 Constant Order Problem

To begin coding these models, we must first use the numerical scheme found in [10] which defines the Caputo fractional derivative of a function $f(t)$. We discretize our domain on a uniform mesh across $[0, T]$ from $n = 1, ..., N$, $\Delta t = \frac{T}{N}$, $t_n = t_0 + n\Delta t$, allowing $f(t_n)$ to be the discretized form of our continuous function $f(t)$. Letting $f(t_n) = f_n$, we have

$$ {}_0^C D_t^\alpha f(t)|_{t=t_n} = \delta_{\Delta t}^\alpha \ f_n + R_n $$

where R_n represents the local truncation error

$$ R_n = \frac{1}{\Gamma(1-\alpha)} \sum_{k=1}^{n} \int_{t_{k-1}}^{t_k} \frac{f_t - (f_k - f_{k-1})}{\Delta t (t_n - \tau)^\alpha} d\tau \tag{3.1} $$

and

$$ \begin{aligned} \delta_{\Delta t}^\alpha \ f_n &= \frac{1}{\Gamma(1-\alpha)} \sum_{k=1}^{n} \int_{t_{k-1}}^{t_k} \frac{f_k - f_{k-1}}{\Delta t (t_n - \tau)^\alpha} d\tau \\ &= \frac{1}{\Gamma(1-\alpha)} \sum_{k=1}^{n} \frac{f_k - f_{k-1}}{\Delta t} \int_{t_{k-1}}^{t_k} \frac{1}{(t_n - \tau)^\alpha} d\tau \\ &= \frac{1}{\Gamma(2-\alpha)} \sum_{k=1}^{n} \frac{[(t_n - t_{k-1})^{1-\alpha} - (t_n - t_k)^{1-\alpha}]}{\Delta t} (f_k - f_{k-1}) \end{aligned} \tag{3.2} $$

Then by incorporating Eq (3.2) into our Eq (2.15) we get Eq (3.3) for our σ_{tot} in terms of our ϵ_{tot} for our constant order Zener Fractional model. Using this discretization with a uniform mesh across $[0, T]$, T our max time and $n = 1, ..., N$, we found the results matched that of the equivalent Generalized Maxwell model based on the results found in [8], the results of which are seen in Chapter 4.

$$
\begin{aligned}
\sigma_{n+1} =& \frac{\beta}{1+\Delta t^{-\alpha}\beta}\left[\sigma_n \Delta t^{-\alpha} - \sum_{k=2}^{n} b_{n,k}(\sigma_k - \sigma_{k-1})\right] \\
&+ \frac{\beta}{1+\Delta t^{-\alpha}\beta}\left[\frac{E_{eq}\epsilon_{n+1}}{\beta} + (E_{eq}+E_{neq})\sum_{k=2}^{n+1} b_{n,k}(\epsilon_k - \epsilon_{k-1})\right] \\
\beta =& \frac{\tau^{\alpha}}{\Gamma(2-\alpha)} \\
b_{n,k} =& \frac{(t_{n+1}-t_{k-1})^{1-\alpha} - (t_{n+1}-t_k)^{1-\alpha}}{\Delta t} \\
\sigma_1 =& 0
\end{aligned}
\tag{3.3}
$$

3.2 Concrete-Variable Order Problem

When modeling the two different aggregate types of concrete based on the experimental data from [2], the values of the α, η clearly change due to different temperatures, which was seen in Table 2.1. Previously Eq's (2.20), (2.21), (2.22) were introduced, and it is with these three different definitions that we will model the creep behavior of the concrete. The discretization process for each along with the numerical scheme are derived in the following subsections.

3.2.1 ${}_0^C D_t^{\alpha} f(t) \Rightarrow {}_0^1 D_t^{\alpha(T(t))} f(t)$

It is clear that the standard constant order definition of the fractional derivative cannot model these, however Eq (3.2) can be easily altered to accommodate this. We do so by discretizing our springpot model chosen for concrete assuming constant stress and our temperature dependent α, setting $\alpha(T(t_n)) = \alpha_n$ for simplicity

$$
\begin{aligned}
{}_0^1 D_t^{\alpha(T(t))} f(t)|_{t=t_n} &\approx \frac{1}{\Gamma(1-\alpha_n)} \sum_{k=1}^{n} \int_{t_{k-1}}^{t_k} \frac{f_k - f_{k-1}}{\Delta t (t_n - \tau)^{\alpha_n}} d\tau \\
&= \frac{1}{\Gamma(1-\alpha_n)} \sum_{k=1}^{n} \frac{f_k - f_{k-1}}{\Delta t} \int_{t_{k-1}}^{t_k} \frac{1}{(t_n - \tau)^{\alpha_n}} d\tau \\
&= \frac{1}{\Gamma(2-\alpha_n)} \sum_{k=1}^{n} \frac{[(t_n - t_{k-1})^{1-\alpha_n} - (t_n - t_k)^{1-\alpha_n}]}{\Delta t} (f_k - f_{k-1})
\end{aligned}
$$

Incorporating this scheme into our Eq (2.18) we get

$$\begin{aligned}\epsilon_n =& \epsilon_{n-1} + \Delta t^{\alpha_n}\Gamma(2-\alpha_n)\frac{\sigma}{\eta_n} \\ &- \sum_{k=2}^{n-1}[(n-k+1)^{1-\alpha_n} - (n-k)^{1-\alpha_n}](\epsilon_k - \epsilon_{k-1}) \\ \epsilon_1 =& 0\end{aligned} \tag{3.4}$$

Here we specifically know what the η values are from Table 2.1 and as such do not need to use our previous definition $\eta = E\tau^{\alpha}$. This discretization was based on our initially known definition of our Caputo fractional derivative found in Eq (2.20), with the only difference being the reliance of how the temperature changes in time, creating an accurate picture of how the model evolves. The coefficient matrix is seen below

$$\begin{bmatrix}\epsilon_2\\ \epsilon_3\\ \epsilon_4\\ \vdots\\ \epsilon_n\end{bmatrix} = \begin{bmatrix}\beta_2\frac{\sigma}{\eta_2} & 0 & \ddots & \cdots & \cdots & 0\\ \beta_3\frac{\sigma}{\eta_3} & 1-c_{3,2} & 0 & \ddots & \cdots & 0\\ \beta_3\frac{\sigma}{\eta_4} & c_{4,3}-c_{4,2} & 1-c_{4,3} & 0 & \ddots & 0\\ \vdots & \vdots & \vdots & \ddots & \ddots & 0\\ \beta_n\frac{\sigma}{\eta_n} & c_{n,3}-c_{n,2} & c_{n,4}-c_{n,3} & \cdots & 1-c_{n,n-1} & 0\end{bmatrix}\begin{bmatrix}1\\ \epsilon_2\\ \epsilon_3\\ \epsilon_4\\ \vdots\\ \epsilon_n\end{bmatrix}$$

where β_n, $c_{n,k}$ are defined as

$$\begin{aligned}\beta_n &= \Delta t^{\alpha_n}\Gamma(2-\alpha_n)\\ c_{n,k} &= (n-k+1)^{1-\alpha_n} - (n-k)^{1-\alpha_n}\end{aligned} \tag{3.5}$$

3.2.2 ${}_0^C D_t^{\alpha} f(t) \Rightarrow {}_0^2 D_t^{\alpha(T(t))} f(t)$

Here we are interested in the discretization of our Eq (2.21), the first step to incorporating memory into our scheme.

$$\begin{aligned}
{}_0^2 D_t^{\alpha(T(t))} f(t)|_{t=t_n} &\approx \sum_{k=2}^{n} \int_{t_{k-1}}^{t_k} \frac{f_k - f_{k-1}}{\Delta t \Gamma(1-\alpha(T(\tau)))(t_n-\tau)^{\alpha(T(\tau))}} d\tau \\
&= \sum_{k=2}^{n} \frac{f_k - f_{k-1}}{\Gamma(1-\alpha_{k-1})\Delta t} \int_{t_{k-1}}^{t_k} \frac{1}{(t_n-\tau)^{\alpha_{k-1}}} d\tau \\
&= \sum_{k=2}^{n} \frac{f_k - f_{k-1}}{\Gamma(2-\alpha_{k-1})\Delta t^{\alpha_{k-1}}} [(n-k+1)^{1-\alpha_{k-1}} - (n-k)^{1-\alpha_{k-1}}]
\end{aligned}$$

From this discretization process of our Eq (2.21) we have our ϵ in terms of our parameters below

$$\begin{aligned}
\epsilon_n &= \epsilon_{n-1} + \Delta t^{\alpha_{n-1}} \Gamma(2-\alpha_{n-1}) \left[\frac{\sigma}{\eta_n} - \sum_{k=2}^{n-1} \frac{\epsilon_k - \epsilon_{k-1}}{\Gamma(2-\alpha_{k-1})\Delta t^{\alpha_{k-1}}} \gamma_{n,k} \right] \\
\gamma_{n,k} &= (n-k+1)^{1-\alpha_{k-1}} - (n-k)^{1-\alpha_{k-1}} \\
\epsilon_1 &= 0
\end{aligned} \tag{3.6}$$

with the coefficient matrix

$$\begin{bmatrix} \epsilon_2 \\ \epsilon_3 \\ \epsilon_4 \\ \vdots \\ \epsilon_n \end{bmatrix} = \begin{bmatrix} \beta_2 \frac{\sigma}{\eta_2} & 0 & \ddots & \cdots & \cdots & 0 \\ \beta_3 \frac{\sigma}{\eta_3} & 1-c_{3,2} & 0 & \ddots & \cdots & 0 \\ \beta_4 \frac{\sigma}{\eta_4} & c_{4,3}-c_{4,2} & 1-c_{4,3} & 0 & \ddots & 0 \\ \vdots & \vdots & \vdots & \ddots & \ddots & 0 \\ \beta_n \frac{\sigma}{\eta_n} & c_{n,3}-c_{n,2} & c_{n,4}-c_{n,3} & \cdots & 1-c_{n,n-1} & 0 \end{bmatrix} \begin{bmatrix} 1 \\ \epsilon_2 \\ \epsilon_3 \\ \epsilon_4 \\ \vdots \\ \epsilon_n \end{bmatrix}$$

and our β_n, $c_{n,k}$ defined as

$$\begin{aligned}
\beta_n &= \Delta t^{\alpha_{n-1}} \Gamma(2-\alpha_{n-1}) \\
c_{n,k} &= \frac{\Delta t^{\alpha_{n-1}} \Gamma(2-\alpha_{n-1})}{\Delta t^{\alpha_{k-1}} \Gamma(2-\alpha_{k-1})} [(n-k+1)^{1-\alpha_{k-1}} - (n-k)^{1-\alpha_{k-1}}]
\end{aligned} \tag{3.7}$$

3.2.3 ${}_0^C D_t^{\alpha} f(t) \Rightarrow {}_0^3 D_t^{\alpha(T(t))} f(t)$

Our final discretization is of Eq (2.22), the final step towards fully integrating memory into our numerical scheme.

$$\begin{aligned}
{}_0^3 D_t^{\alpha(T(t))} f(t)|_{t=t_n} &\approx \sum_{k=2}^{n} \int_{t_{k-1}}^{t_k} \frac{f_k - f_{k-1}}{\Delta t \Gamma(1-\alpha(T(t_n-\tau)))(t_n-\tau)^{\alpha(T(t_n-\tau))}} d\tau \\
&= \sum_{k=2}^{n} \frac{f_k - f_{k-1}}{\Gamma(1-\alpha_{n-k+1})\Delta t} \int_{t_{k-1}}^{t_k} \frac{1}{(t_n-\tau)^{\alpha_{n-k+1}}} d\tau \\
&= \sum_{k=2}^{n} \frac{f_k - f_{k-1}}{\Gamma(2-\alpha_{n-k+1})\Delta t^{\alpha_{n-k+1}}} [(n-k+1)^{1-\alpha_{n-k+1}} - (n-k)^{1-\alpha_{n-k+1}}]
\end{aligned}$$

With this final numerical scheme for our Eq (2.22), we can find our ϵ in terms of our parameters below

$$\begin{aligned}
\epsilon_n &= \epsilon_{n-1} + \Delta t^{\alpha_1} \Gamma(2-\alpha_1) \left[\frac{\sigma}{\eta_n} - \sum_{k=2}^{n-1} \frac{\epsilon_k - \epsilon_{k-1}}{\Gamma(2-\alpha_{n-k+1})\Delta t^{\alpha_{n-k+1}}} \gamma_{n,k} \right] \\
\gamma_{n,k} &= (n-k+1)^{1-\alpha_{n-k+1}} - (n-k)^{1-\alpha_{n-k+1}} \\
\epsilon_1 &= 0
\end{aligned} \tag{3.8}$$

and our coefficient matrix

$$\begin{bmatrix} \epsilon_2 \\ \epsilon_3 \\ \epsilon_4 \\ \vdots \\ \epsilon_n \end{bmatrix} = \begin{bmatrix} \beta\frac{\sigma}{\eta_2} & 0 & \ddots & \cdots & \cdots & 0 \\ \beta\frac{\sigma}{\eta_3} & 1-c_{3,2} & 0 & \ddots & \cdots & 0 \\ \beta\frac{\sigma}{\eta_4} & c_{4,3}-c_{4,2} & 1-c_{4,3} & 0 & \ddots & 0 \\ \vdots & \vdots & \vdots & \ddots & \ddots & 0 \\ \beta\frac{\sigma}{\eta_n} & c_{n,3}-c_{n,2} & c_{n,4}-c_{n,3} & \cdots & 1-c_{n,n-1} & 0 \end{bmatrix} \begin{bmatrix} 1 \\ \epsilon_2 \\ \epsilon_3 \\ \epsilon_4 \\ \vdots \\ \epsilon_n \end{bmatrix}$$

with our β, $c_{n,k}$ defined as

$$\begin{aligned}
\beta &= \Delta t^{\alpha_1} \Gamma(2-\alpha_1) \\
c_{n,k} &= \frac{\Delta t^{\alpha_1} \Gamma(2-\alpha_1)}{\Delta t^{\alpha_{n-k+1}} \Gamma(2-\alpha_{n-k+1})} [(n-k+1)^{1-\alpha_{n-k+1}} - (n-k)^{1-\alpha_{n-k+1}}]
\end{aligned} \tag{3.9}$$

3.2.4 Difference in Coefficient Matrices

While the process for each case resulted in similar coefficient matrices, the clear difference lies in the coefficients themselves. For Eq (3.5), for each n step, the α_n was only evaluated at n for each summation step, essentially acting as a constant for each iteration. However for Eq (3.7), α is distinctly dependent upon either the k'th or n'th iteration, seen in α_{k-1} or α_{n-1}. While this allows the α values to mature throughout the iterative process providing that sense of memory, it is only dependent upon which iteration it is being processed as, and as such has no dependence upon the t_n value in which it is being derived with respect to except at $k = n$. Finally in Eq (3.9) we see the α evaluated based upon an interactive relationship between both the k'th and n'th value. This allows the scheme as a whole to preserve the memory of the α function with respect to both the iterative process as well as the t_n values.

Chapter 4

Numerical Experiments

4.1 Convergence Behavior

To check the accuracy of our numerical scheme from Eq (3.2) we discretized the differential equation $(1+t^2)f'(t) + {}_0^C D_t^{0.1+0.2^{\sqrt{t}}} f(t) = f(t)$ against its true solution $f(t) = 1 + t^{1.7}$, seen below

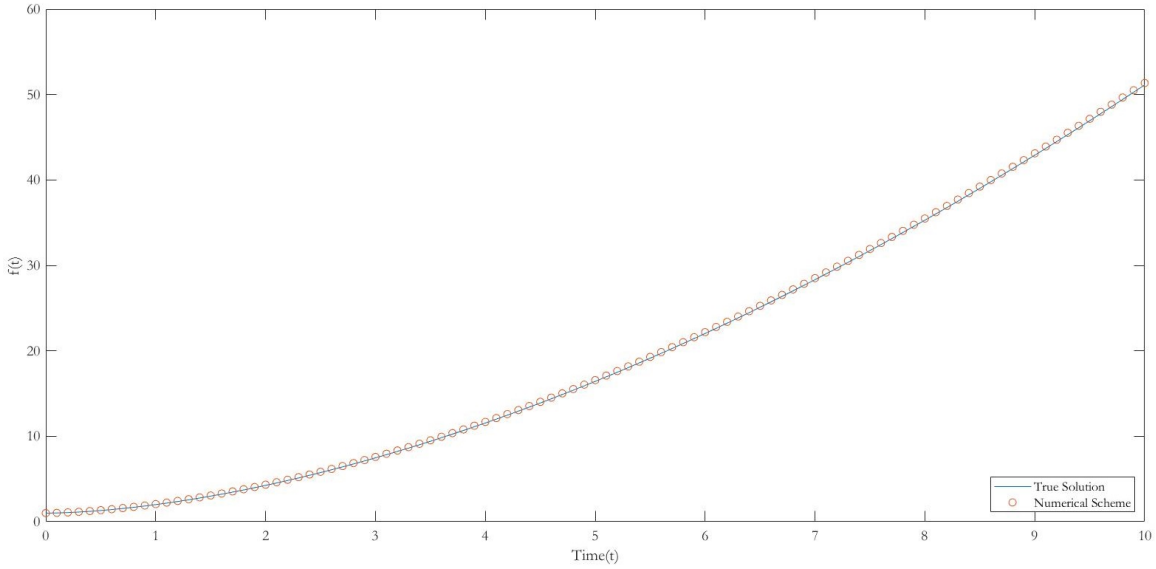

Figure 4.1: Equivalence between our numerical scheme and the true solution

In Fig: 4.1 it can be seen that the code written using the numerical scheme aligns closely to the true solution. The error and Newton Convergence Order were then calculated and the results can be seen in Table 4.1, with $e_n = ||f - f_n||_{L_\infty}$, β_n representing the convergence order, and N the iterations. With these results we were able to move forward confidently with incorporating the numerical scheme to model viscoelastic materials.

Table 4.1: Error and Newton Convergence Order of Eq (3.2)

N	Δt	e_n	β_n
32	$\frac{1}{32}$	0.0187	99.08%
64	$\frac{1}{64}$	0.0094	99.46%
128	$\frac{1}{128}$	0.0047	99.68%
256	$\frac{1}{256}$	0.0024	99.81%
512	$\frac{1}{512}$	0.0012	99.88%
1024	$\frac{1}{1024}$	0.0006	99.93%

4.2 Numerical Investigation of Fractional Zener model compared to Generalized Maxwell model

With our Eq (3.3), we can now verify it against known results. In [8] they compare the equivalence of a Fractional Zener model (Fig: 2.3) against the Generalized Maxwell model (Fig: 2.2). Using the values in the paper with E_{eq} set to 1MPa, E_{neq} set to 999MPa, we ran the code through a series of tests seen in Fig: 4.2 to see if we could replicate the results.

The first test we ran was a stress response-we set the strain to increase at a constant rate of 0.01/s, 0.001/s, and 0.0001/s with results seen in Fig: 4.2(a). The second test we ran was stress relaxation, where the strain was increased to either 0.01, 0.03, or 0.05 and then held at that level for 60s, as seen in Fig: 4.2(b). The third and final test we conducted was under cyclic loading conditions, where the strain over time can be seen in Fig: 4.2(c) with resulting stress response Fig: 4.2(d). Comparing these results to those found in [8], we were able to confirm the validity of Eq (3.3) and also prove that while modeling viscoelastic materials is possible using integer order derivatives as seen in our Generalized Maxwell model in Eq (2.6), it is much simpler to use a fractional model such as our Fractional Zener model.

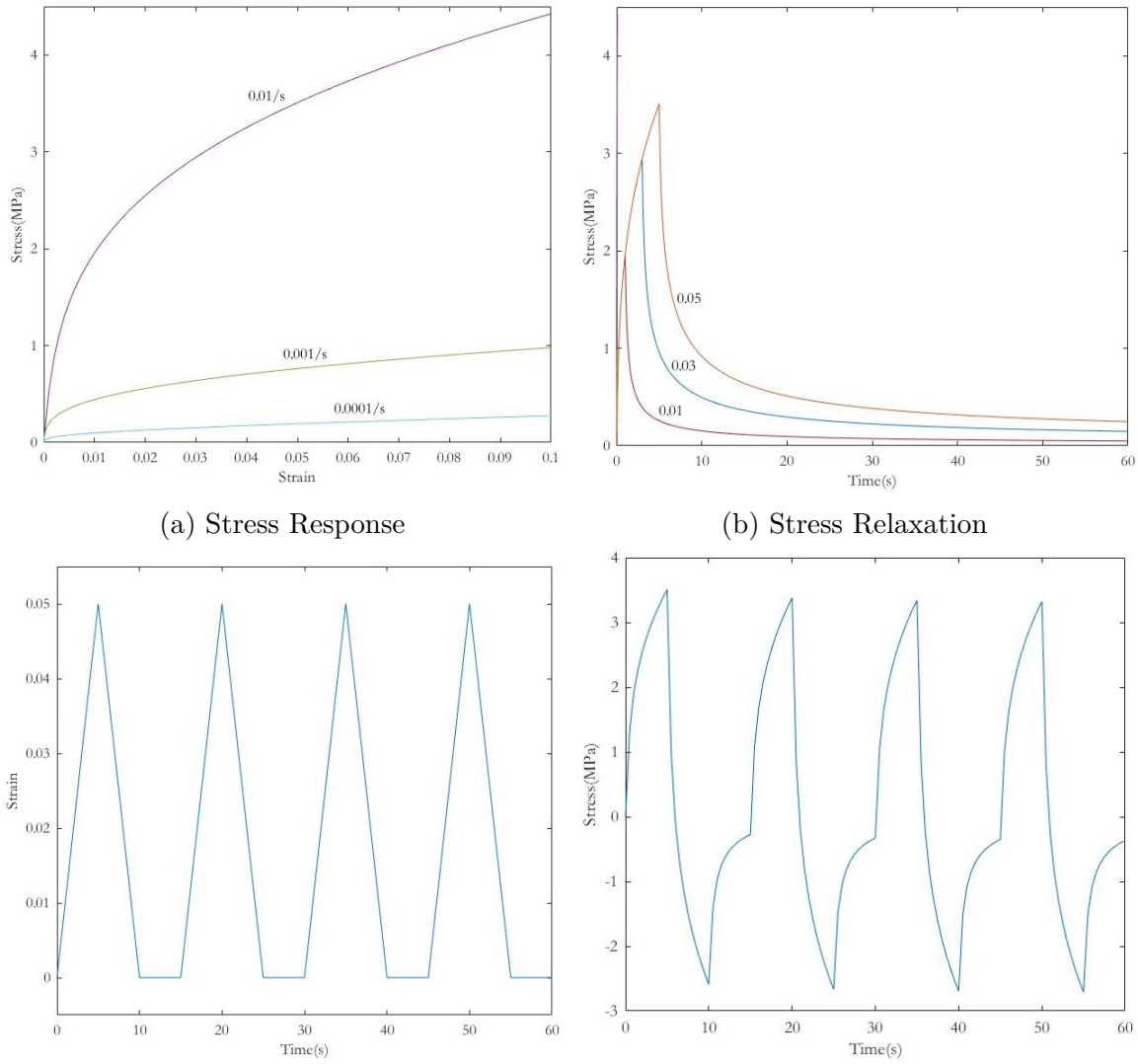

(a) Stress Response

(b) Stress Relaxation

(c) Cyclic Loading-Strain

(d) Cyclic Loading-Stress

Figure 4.2: The results of our Fractional Zener model subject to three different loading conditions with ω=0.1, α=0.7

Comparing the two equations it is quite clear that Eq (3.3) is advantageous due to its minimal unknowns, while Eq (2.6) require many unknowns making the computation lengthier.

4.3 Exploring our Impulse Function

To discover how the different definitions from Eq's (3.4), (3.8), and (3.6) differ from each other, a closer look at the impulse function of each provides clarity. Here we graphed the impulse function for each with τ our integration variable, and t the value the derivative is being taken with respect to. Our t values start at 35 minutes and increment by 35 until 350 minutes, represented by the separate graphs seen in Fig:'s 4.4, 4.5, 4.6. This is in the effort to show how the discretization of the function is affected as our t_n increases. For reference Fig: 4.3 displays the temperature dependent α values.

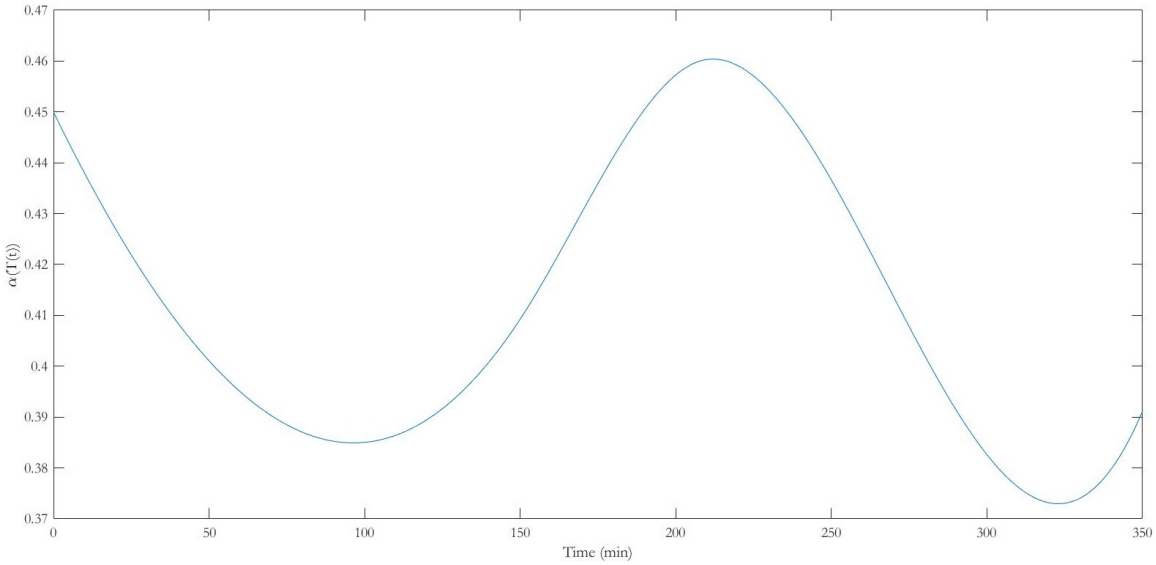

Figure 4.3: MATLAB spline function of α parameters found in Table 2.1

4.3.1 Eq (2.20) Impulse Function

As described earlier the α function acts as a constant, and this is represented in the initial values of each t_n impulse function graph seen in Fig: 4.4. Each behaves as an independent graph regardless of how α changes in time according to our Fig: 4.3.

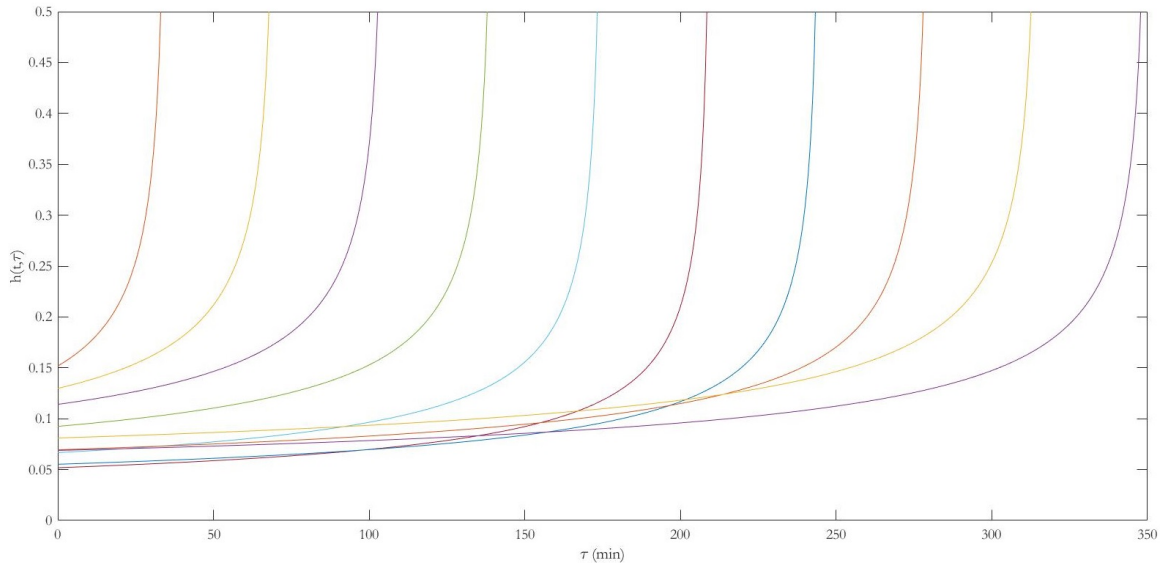

Figure 4.4: Our impulse function using $\alpha(T(t,\tau)) \Rightarrow \alpha(T(t))$

4.3.2 Eq (2.21) Impulse Function

However here we have the α dependent upon each value within the k'th iteration, seen in how the beginning of the t_n graphs in Fig: 4.5 behaves compared to Fig: 4.4. There is simultaneous oscillation reflecting our α values as our τ increments from 0 min to 350 min, similar to the α behavior in Fig: 4.3.

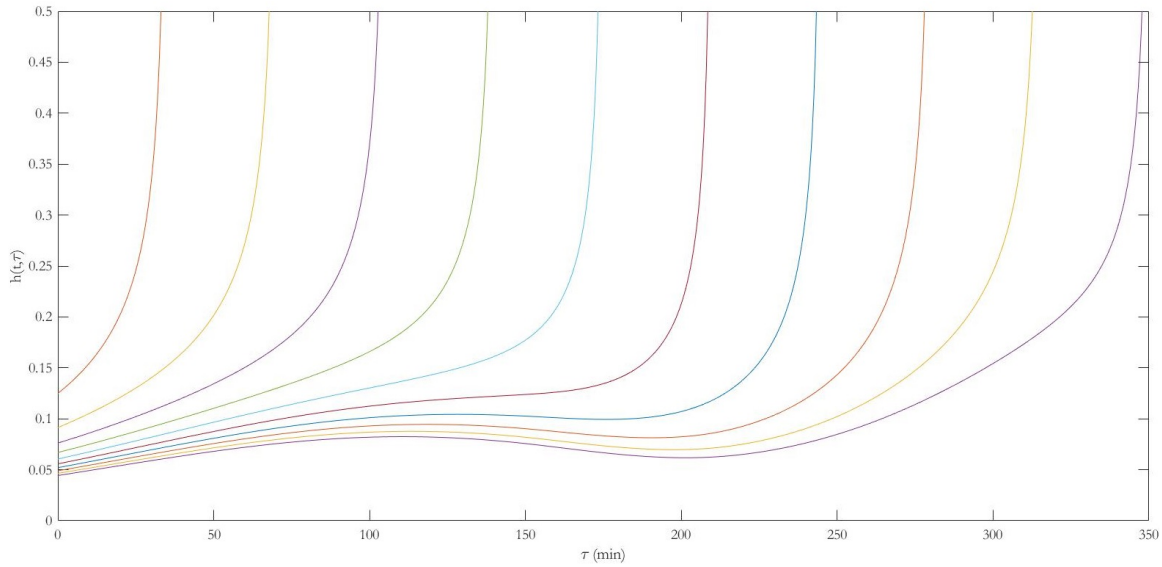

Figure 4.5: Our impulse function using $\alpha(T(t,\tau)) \Rightarrow \alpha(T(\tau))$

4.3.3 Eq (2.22) Impulse Function

Finally we have our impulse function from our third definition. From Eq (3.9) we could clearly see an interactive relationship between our t_n, τ values and this is reflected in the distinct oscillations at the beginning of each t_n graph found in Fig: 4.6. The distinct behavior of these graphs clearly show that our Eq (2.22) allows much greater respect to how the α function evolves as t_n increases respective to Fig: 4.3.

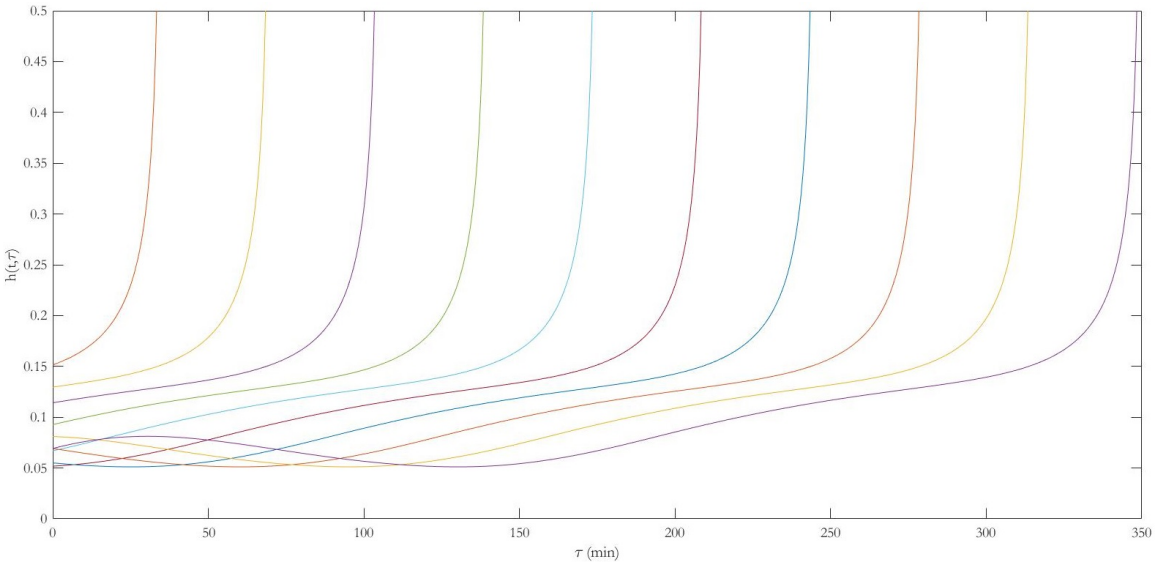

Figure 4.6: Our impulse function using $\alpha(T(t,\tau)) \Rightarrow \alpha(T(t-\tau))$

4.4 Numerical Investigation of Concrete

Here we wanted to compare our three equations defined in Eq's (2.20), (2.21), and (2.22). We focused on calcareous and siliceous aggregate which behaved quite differently when subjected to different temperatures. To model calcareous aggregate using Eq's (3.4), (3.6), and (3.8), we used Eq (2.16), however as seen in Fig: 4.7(a), it was clear that there was an issue with the equations around the time 150min, which correlates to 600°F as seen in Fig: 4.7(b) where there is jump discontinuity in the α equation.

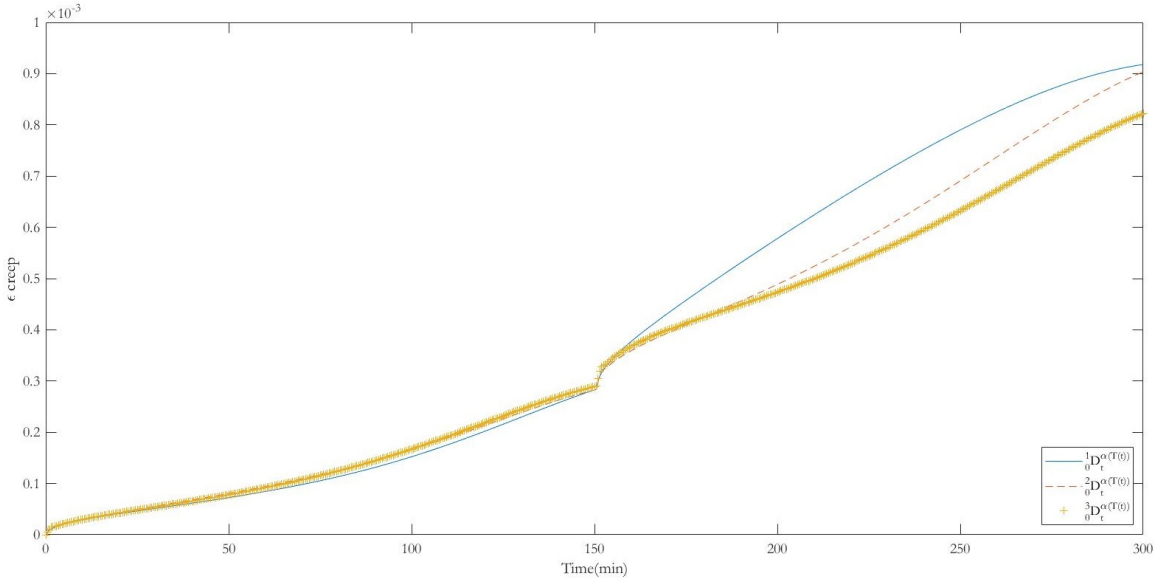

(a) Calcareous aggregate creep

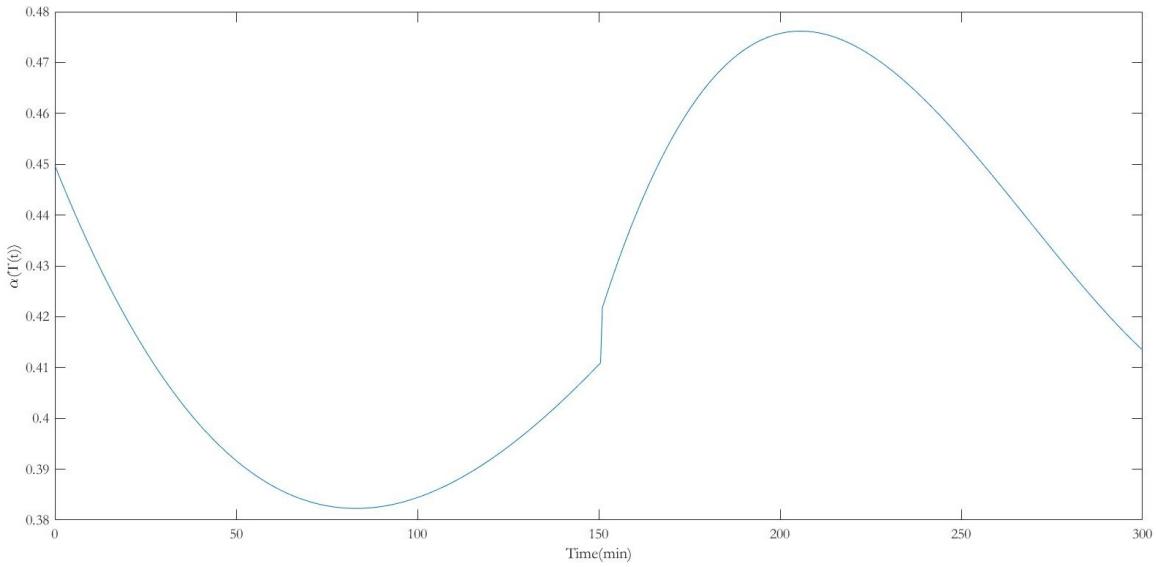

(b) Calcareous α(T(t)) values

Figure 4.7: Calcareous aggregate creep and $\alpha(T(t))$ based on Eq (2.16)

Seeing how the α function jumps at $t_n = 150$min we chose to graph the values from Table 2.1 directly using the MATLAB spline function, seen in Fig: 4.8. Here it is plain that the discretization in Eq's (3.6) and (3.8) produces a smoother graph-consistent with the notion that it takes the history of the evolution of α into account in the direct calculations of the fractional derivative of the springpot.

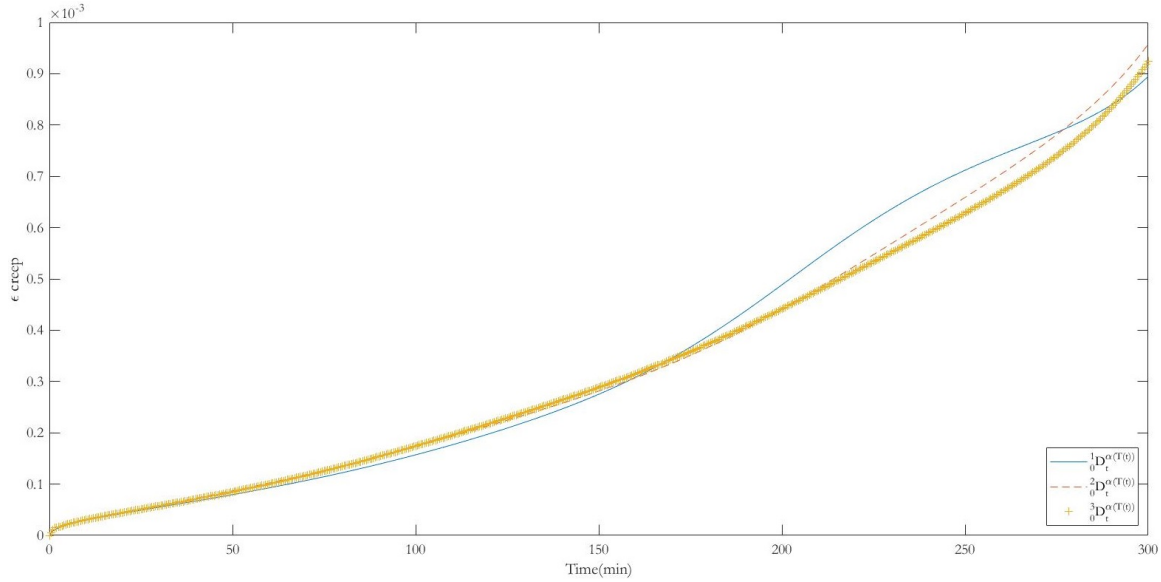

Figure 4.8: Calcareous aggregate creep using MATLAB spline function for parameters found in Table 2.1

Conversely comparing the graphs that result from using the equations for α, η found in Eq (2.17) to those found using a direct MATLAB spline function from the parameters for siliceous aggregate found in Table 2.1, there was little difference to note except a slight scaling factor due to slightly enlarged values of the α, η graphs from Eq (2.17).

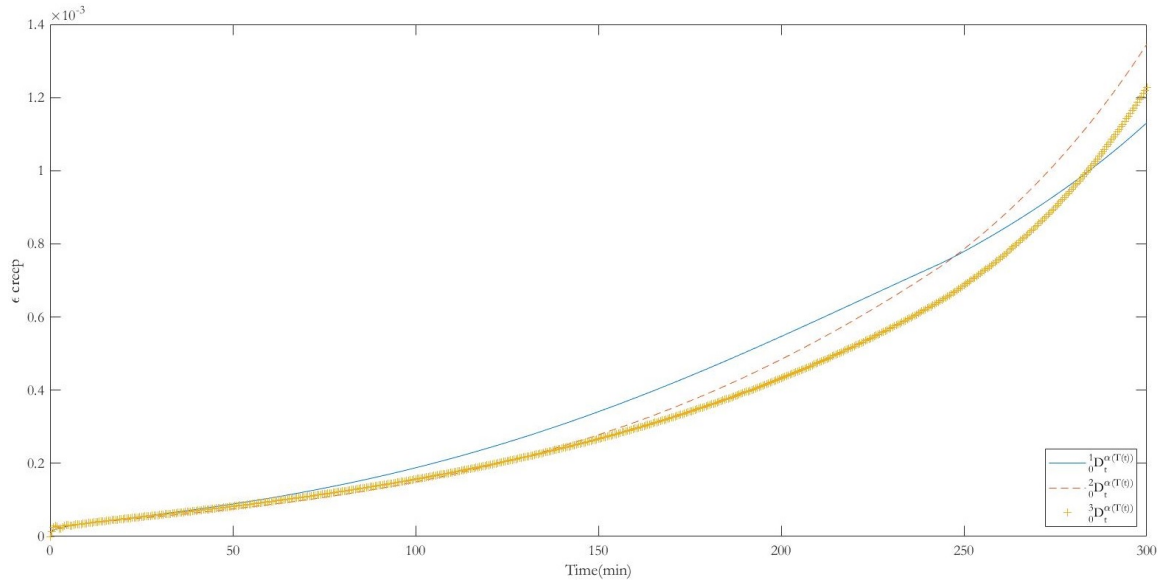

Figure 4.9: Siliceous aggregate creep based on Eq (2.17)

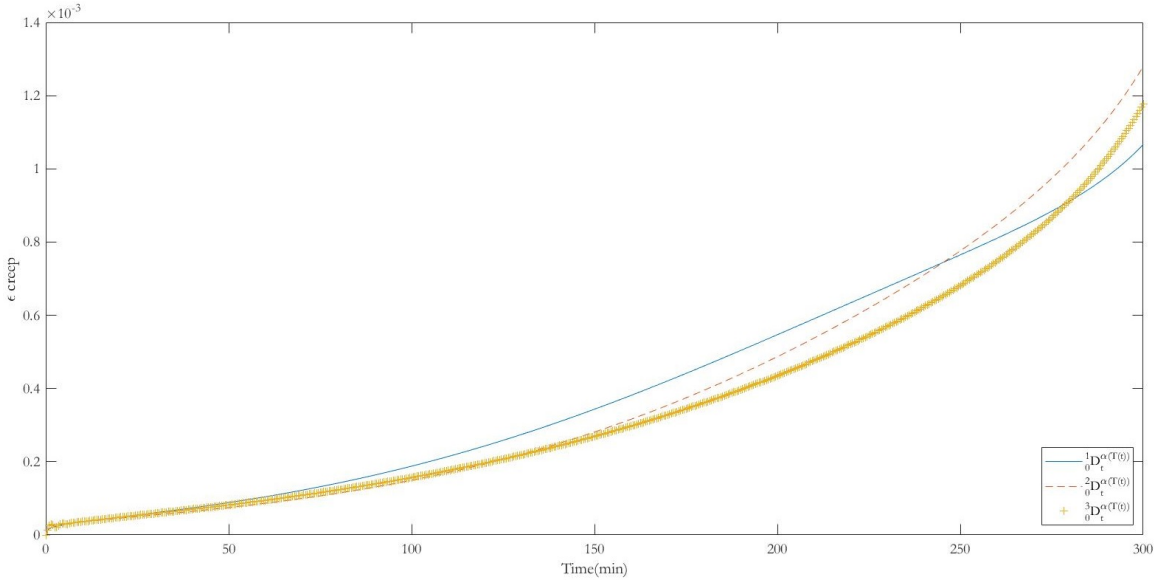

Figure 4.10: Siliceous aggregate creep using MATLAB spline function for parameters found in Table 2.1

Some things to note include how the first definition of our Caputo derivative produces graphs that rely heavily on the α function calculated at t_n, seen in the initial increase in values followed by a tail end of decreasing values compared to our other definitions. However looking at our second and third definitions we can see a clearer evolution with respect to the α functions given the smoother increase in our function as time progresses forward.

Chapter 5

Conclusion and Future Work

In this thesis we have successfully shown that fractional order viscoelastic models have a clear advantage to modeling such materials specifically in contrasting the numerical schemes required for a Generalized Maxwell model and the Fractional Zener model. From this we verified the numerical scheme initially introduced, providing a 99%+ convergence order for minimal iterations, to which we applied to a variable order α function definition to different types of concrete aggregate. To discover how the implementation of varying the relationship between our integration variable τ to our t with which we took the derivative with respect to within the α function, we introduced our three different definitions ${}_0^1D_t^{\alpha(T(t))}f(t)$, ${}_0^2D_t^{\alpha(T(t))}f(t)$, and ${}_0^3D_t^{\alpha(T(t))}f(t)$ which we applied to the concrete aggregates. By focusing on the impulse functions defined from our different definitions we discussed how each differed in respect to another, specifically how the numerical scheme of each allowed more or less contribution from our α function dependent upon which time stamp in the iterative process.

From here more work can be done exploring these different types of definitions, including the acquirement of raw data that can be modeled using these definitions to create better approximations of how viscoelastic materials behave, allowing them to be used in broader fields of industry with more confidence.

Bibliography

[1] A. Atangana. *Derivative with a New Parameter*, Academic Press, London, (2016).

[2] Y. Bouras, D. Zorica, T. M. Atanacković and Z. Vrcelj. A non-linear thermo-viscoelastic rheological model based on fractional derivatives for high temperature creep in concrete. *Applied Mathematical Modelling* 55 (2018), 551–568.

[3] P. Haupt, A. Lion and E. Backhaus. On the dynamic behaviour of polymers under finite strains: constitutive modelling and identification of parameters. *International Journal of Solids and Structures* 37 (2000), 3633–3646.

[4] Z. Li, H. Wang, R. Xiao and S. Yang. A variable-order fractional differential equation model of shape memory polymers. *Chaos, Solitons & Fractals* 102 (2017), 473–485.

[5] C. F. Lorenzo and T. T. Hartley. Variable Order and Distributed Order Fractional Operators. *Nonlinear Dynamics* 29 (2002), 57–98.

[6] I. Podlubny. *Fractional Differential Equations*, Academic Press, California, (1999).

[7] R. Xiao, J. Choi, N. Lakhera, C. M. Yakacki, C. P. Frick and T. D. Nguyen. Modeling the glass transition of amorphous networks for shape-memory behavior. *Journal of the Mechanics and Physics of Solids* 62 (2013), 1612–1635.

[8] R. Xiao, H. Sun and W. Chen. An equivalence between generalized Maxwell model and fractional Zener model. *Mechanics of Materials* 100 (2016), 148–153.

[9] Z. Yang, X. Zheng and H. Wang. An indirect collocation method for variable-order fractional wave equations on uniform or graded meshes and its optimal error estimates. *International Journal of Computer Mathematics* 00 (2021), 1–14.

[10] X. Zheng and H. Wang. Optimal-order error estimates of finite element approximations to variable-order time-fractional diffusion equations without regularity

assumptions of the true solutions. *IMA Journal of Numerical Analysis* 00 (2020), 1–24.